X-Ray Polarization Observations of BL Lacertae

Riccardo Middei, Ioannis Liodakis, Matteo Perri, Simonetta Puccetti, Elisabetta Cavazzuti, Laura Di Gesu, Steven R. Ehlert, Grzegorz Madejski, Alan P. Marscher, Herman L. Marshall, et al.

The Astrophysical Journal Letters, 942:L10 (14pp), 2023 January 1 https://doi.org/10.3847/2041-8213/aca281

X-Ray Polarization Observations of BL Lacertae

Riccardo Middei[1,2], Ioannis Liodakis[3], Matteo Perri[1,2], Simonetta Puccetti[1], Elisabetta Cavazzuti[4], Laura Di Gesu[4], Steven R. Ehlert[5], Grzegorz Madejski[6], Alan P. Marscher[7], Herman L. Marshall[8], Fabio Muleri[9], Michela Negro[10,11], Svetlana G. Jorstad[7,12], Beatriz Agís-González[13], Iván Agudo[13], Giacomo Bonnoli[13,14], Maria I. Bernardos[13], Víctor Casanova[13], Maya García-Comas[13], César Husillos[13], Alessandro Marchini[15], Alfredo Sota[13], Pouya M. Kouch[3,16], Elina Lindfors[3], George A. Borman[17], Evgenia N. Kopatskaya[12], Elena G. Larionova[12], Daria A. Morozova[12], Sergey S. Savchenko[12,18,19], Andrey A. Vasilyev[12], Alexey V. Zhovtan[17], Carolina Casadio[20,21], Juan Escudero[13], Ioannis Myserlis[22], Antonio Hales[23,24], Seiji Kameno[25,26], Ruediger Kneissl[27,28], Hugo Messias[23], Hiroshi Nagai[29,30], Dmitry Blinov[20], Ioakeim G. Bourbah[21], Sebastian Kiehlmann[20,21], Evangelos Kontopodis[21], Nikos Mandarakas[20,21], Stylianos Romanopoulos[20,21], Raphael Skalidis[20,21], Anna Vervelaki[21], Joseph R. Masiero[31], Dimitri Mawet[32], Maxwell A. Millar-Blanchaer[33], Georgia V. Panopoulou[34], Samaporn Tinyanont[35], Andrei V. Berdyugin[16], Masato Kagitani[36], Vadim Kravtsov[16], Takeshi Sakanoi[36], Ryo Imazawa[37], Mahito Sasada[38], Yasushi Fukazawa[37,39,40], Koji S. Kawabata[37,39,40], Makoto Uemura[37,39,40], Tsunefumi Mizuno[39], Tatsuya Nakaoka[39], Hiroshi Akitaya[41], Mark Gurwell[42], Ramprasad Rao[42], Niccoló Di Lalla[6], Nicoló Cibrario[43], Immacolata Donnarumma[4], Dawoon E. Kim[9,44,45], Nicola Omodei[6], Luigi Pacciani[9], Juri Poutanen[16,46], Fabrizio Tavecchio[14], Lucio A. Antonelli[1,2], Matteo Bachetti[47], Luca Baldini[48,49], Wayne H. Baumgartner[5], Ronaldo Bellazzini[48], Stefano Bianchi[50], Stephen D. Bongiorno[5], Raffaella Bonino[51,52], Alessandro Brez[48], Niccoló Bucciantini[53,54,55], Fiamma Capitanio[9], Simone Castellano[48], Stefano Ciprini[1,56], Enrico Costa[9], Alessandra De Rosa[9], Ettore Del Monte[9], Alessandro Di Marco[9], Victor Doroshenko[57], Michal Dovčiak[58], Teruaki Enoto[59], Yuri Evangelista[9], Sergio Fabiani[9], Riccardo Ferrazzoli[9], Javier A. Garcia[60], Shuichi Gunji[61], Kiyoshi Hayashida[62], Jeremy Heyl[63], Wataru Iwakiri[64], Vladimir Karas[58], Takao Kitaguchi[59], Jeffery J. Kolodziejczak[5], Henric Krawczynski[65], Fabio La Monaca[9], Luca Latronico[51], Simone Maldera[51], Alberto Manfreda[48], Frédéric Marin[66], Andrea Marinucci[4], Francesco Massaro[51,52], Giorgio Matt[50], Ikuyuki Mitsuishi[67], C.-Y. Ng[68], Stephen L. O'Dell[5], Chiara Oppedisano[51], Alessandro Papitto[2], George G. Pavlov[69], Abel L. Peirson[6], Melissa Pesce-Rollins[48], Pierre-Olivier Petrucci[70], Maura Pilia[47], Andrea Possenti[47], Brian D. Ramsey[5], John Rankin[9], Ajay Ratheesh[9], Roger W. Romani[6], Carmelo Sgró[48], Patrick Slane[71], Paolo Soffitta[9], Gloria Spandre[48], Toru Tamagawa[59], Roberto Taverna[72], Yuzuru Tawara[67], Allyn F. Tennant[5], Nicholas E. Thomas[5], Francesco Tombesi[45,56,73], Alessio Trois[47], Sergey Tsygankov[16,46], Roberto Turolla[72,74], Jacco Vink[75], Martin C. Weisskopf[5], Kinwah Wu[74], Fei Xie[9,76], and Silvia Zane[74]

[1] Space Science Data Center, Agenzia Spaziale Italiana, Via del Politecnico snc, I-00133 Roma, Italy; riccardo.middei@ssdc.asi.it
[2] INAF Osservatorio Astronomico di Roma, Via Frascati 33, I-00078 Monte Porzio Catone (RM), Italy
[3] Finnish Centre for Astronomy with ESO, FI-20014 University of Turku, Finland
[4] ASI—Agenzia Spaziale Italiana, Via del Politecnico snc, I-00133 Roma, Italy
[5] NASA Marshall Space Flight Center, Huntsville, AL 35812, USA
[6] Department of Physics and Kavli Institute for Particle Astrophysics and Cosmology, Stanford University, Stanford, CA 94305, USA
[7] Institute for Astrophysical Research, Boston University, 725 Commonwealth Avenue, Boston, MA 02215, USA
[8] MIT Kavli Institute for Astrophysics and Space Research, Massachusetts Institute of Technology, 77 Massachusetts Avenue, Cambridge, MA 02139, USA
[9] INAF Istituto di Astrofisica e Planetologia Spaziali, Via del Fosso del Cavaliere 100, I-00133 Roma, Italy
[10] University of Maryland, Baltimore County, Baltimore, MD 21250, USA
[11] Center for Research and Exploration in Space Science and Technology, NASA Goddard Space Flight Center, Greenbelt, MD 20771, USA
[12] Astronomical Institute, St. Petersburg State University, 28 Universitetsky prospekt, Peterhof, St. Petersburg, 198504, Russia
[13] Instituto de Astrofísica de Andalucía-CSIC, Glorieta de la Astronomía s/n, E-18008, Granada, Spain
[14] INAF Osservatorio Astronomico di Brera, Via E. Bianchi 46, I-23807 Merate (LC), Italy
[15] Astronomical Observatory, Department of Physical Sciences, Earth and Environment, University of Siena, Via Roma 56, I-53100 Siena, Italy
[16] Department of Physics and Astronomy, University of Turku, FI-20014, Finland
[17] Crimean Astrophysical Observatory RAS, P/O Nauchny, 298409, Crimea[†]
[18] Special Astrophysical Observatory, Russian Academy of Sciences, 369167, Nizhnii Arkhyz, Russia
[19] Pulkovo Observatory, St.Petersburg, 196140, Russia
[20] Institute of Astrophysics, Foundation for Research and Technology-Hellas, GR-71110 Heraklion, Greece
[21] Department of Physics, University of Crete, GR-70013, Heraklion, Greece
[22] Institut de Radioastronomie Millimétrique, Avenida Divina Pastora, 7, Local 20, E-18012 Granada, Spain
[23] Joint ALMA Observatory, Alonso de Cordova 3107, Vitacura 763-0355, Santiago de Chile, Chile
[24] National Radio Astronomy Observatory, 520 Edgemont Road, Charlottesville, VA 22903-2475, USA
[25] Joint ALMA Observatory, Alonso de Cordova 3107 Vitacura, Santiago 763-0355, Chile
[26] NAOJ Chile Observatory, Alonso de Cordova 3788, Oficina 61B, Vitacura, Santiago, Chile
[27] European Southern Observatory, ESO Vitacura, Alonso de Cordova 3107, Vitacura, Casilla, 19001 Santiago, Chile
[28] Atacama Large Millimeter/submillimeter Array, ALMA Santiago Central Offices, Alonso de Cordova 3107, Vitacura, Casilla, 763-0355 Santiago, Chile
[29] National Astronomical Observatory of Japan, 2-21-1 Osawa, Mitaka, Tokyo 181-8588, Japan
[30] Department of Astronomical Science, The Graduate University for Advanced Studies (SOKENDAI), 2-21-1 Osawa, Mitaka, Tokyo 181-8588, Japan
[31] Caltech/IPAC, 1200 East California Boulevard, MC 100-22, Pasadena, CA 91125, USA
[32] California Institute of Technology, MC 249-17, 1200 East California Boulevard, Pasadena, CA, 91125, USA
[33] Department of physics, University of California, Santa Barbara, CA 93106, USA
[34] California Institute of Technology, MC 350-17, 1200 East California Boulevard, Pasadena, CA, 91125, USA

[35] University of California Santa Cruz, 1156 High Street, Santa Cruz, CA 95064 USA
[36] Graduate School of Sciences, Tohoku University, Aoba-ku, 980-8578 Sendai, Japan
[37] Department of Physics, Graduate School of Advanced Science and Engineering, Hiroshima University Kagamiyama, 1-3-1 Higashi-Hiroshima, Hiroshima 739-8526, Japan
[38] Department of Physics, Tokyo Institute of Technology, 2-12-1 Ookayama, Meguro-ku, Tokyo 152-8551, Japan
[39] Hiroshima Astrophysical Science Center, Hiroshima University 1-3-1 Kagamiyama, Higashi-Hiroshima, Hiroshima 739-8526, Japan
[40] Core Research for Energetic Universe (Core-U), Hiroshima University, 1-3-1 Kagamiyama, Higashi-Hiroshima, Hiroshima 739-8526, Japan
[41] Planetary Exploration Research Center, Chiba Institute of Technology 2-17-1 Tsudanuma, Narashino, Chiba 275-0016, Japan
[42] Center for Astrophysics — Harvard & Smithsonian, 60 Garden Street, Cambridge, MA 02138 USA
[43] Dipartimento di Fisica, Universitá degli Studi di Torino, Via Pietro Giuria 1, I-10125 Torino, Italy
[44] Dipartimento di Fisica, Università degli Studi di Roma "La Sapienza," Piazzale Aldo Moro 5, I-00185 Roma, Italy
[45] Dipartimento di Fisica, Università degli Studi di Roma "Tor Vergata," Via della Ricerca Scientifica 1, 00133 Roma, Italy
[46] Space Research Institute of the Russian Academy of Sciences, Profsoyuznaya Str. 84/32, Moscow 117997, Russia
[47] INAF Osservatorio Astronomico di Cagliari, Via della Scienza 5, I-09047 Selargius (CA), Italy
[48] Istituto Nazionale di Fisica Nucleare, Sezione di Pisa, Largo B. Pontecorvo 3, I-56127 Pisa, Italy
[49] Dipartimento di Fisica, Università di Pisa, Largo B. Pontecorvo 3, I-56127 Pisa, Italy
[50] Dipartimento di Matematica e Fisica, Università degli Studi Roma Tre, Via della Vasca Navale 84, I-00146 Roma, Italy
[51] Istituto Nazionale di Fisica Nucleare, Sezione di Torino, Via Pietro Giuria 1, I-10125 Torino, Italy
[52] Dipartimento di Fisica, Università degli Studi di Torino, Via Pietro Giuria 1, I-10125 Torino, Italy
[53] INAF Osservatorio Astrofisico di Arcetri, Largo Enrico Fermi 5, I-50125 Firenze, Italy
[54] Dipartimento di Fisica e Astronomia, Università degli Studi di Firenze, Via Sansone 1, I-50019 Sesto Fiorentino (FI), Italy
[55] Istituto Nazionale di Fisica Nucleare, Sezione di Firenze, Via Sansone 1, I-50019 Sesto Fiorentino (FI), Italy
[56] Istituto Nazionale di Fisica Nucleare, Sezione di Roma "Tor Vergata", Via della Ricerca Scientifica 1, I-00133 Roma, Italy
[57] Institut für Astronomie und Astrophysik, Universität Tübingen, Sand 1, D-72076 Tübingen, Germany
[58] Astronomical Institute of the Czech Academy of Sciences, Boční II 1401/1, 14100 Praha 4, Czech Republic
[59] RIKEN Cluster for Pioneering Research, 2-1 Hirosawa, Wako, Saitama 351-0198, Japan
[60] California Institute of Technology, Pasadena, CA 91125, USA
[61] Yamagata University,1-4-12 Kojirakawa-machi, Yamagata-shi 990-8560, Japan
[62] Osaka University, 1-1 Yamadaoka, Suita, Osaka 565-0871, Japan
[63] University of British Columbia, Vancouver, BC V6T 1Z4, Canada
[64] Department of Physics, Faculty of Science and Engineering, Chuo University, 1-13-27 Kasuga, Bunkyo-ku, Tokyo 112-8551, Japan
[65] Physics Department and McDonnell Center for the Space Sciences, Washington University in St. Louis, St. Louis, MO 63130, USA
[66] Université de Strasbourg, CNRS, Observatoire Astronomique de Strasbourg, UMR 7550, F-67000 Strasbourg, France
[67] Graduate School of Science, Division of Particle and Astrophysical Science, Nagoya University, Furo-cho, Chikusa-ku, Nagoya, Aichi 464-8602, Japan
[68] Department of Physics, The University of Hong Kong, Pokfulam, Hong Kong
[69] Department of Astronomy and Astrophysics, Pennsylvania State University, University Park, PA 16802, USA
[70] Université Grenoble Alpes, CNRS, IPAG, F-38000 Grenoble, France
[71] Center for Astrophysics — Harvard & Smithsonian, 60 Garden Street, Cambridge, MA 02138, USA
[72] Dipartimento di Fisica e Astronomia, Università degli Studi di Padova, Via Marzolo 8, I-35131 Padova, Italy
[73] Department of Astronomy, University of Maryland, College Park, Maryland 20742, USA
[74] Mullard Space Science Laboratory, University College London, Holmbury St Mary, Dorking, Surrey RH5 6NT, UK
[75] Anton Pannekoek Institute for Astronomy & GRAPPA, University of Amsterdam, Science Park 904, 1098 XH Amsterdam, The Netherlands
[76] Guangxi Key Laboratory for Relativistic Astrophysics, School of Physical Science and Technology, Guangxi University, Nanning 530004, People's Republic of China

Received 2022 October 26; revised 2022 November 11; accepted 2022 November 14; published 2022 December 28

Abstract

Blazars are a class of jet-dominated active galactic nuclei with a typical double-humped spectral energy distribution. It is of common consensus that the synchrotron emission is responsible for the low frequency peak, while the origin of the high frequency hump is still debated. The analysis of X-rays and their polarization can provide a valuable tool to understand the physical mechanisms responsible for the origin of high-energy emission of blazars. We report the first observations of BL Lacertae (BL Lac) performed with the Imaging X-ray Polarimetry Explorer, from which an upper limit to the polarization degree $\Pi_X < 12.6\%$ was found in the 2–8 keV band. We contemporaneously measured the polarization in radio, infrared, and optical wavelengths. Our multiwavelength polarization analysis disfavors a significant contribution of proton-synchrotron radiation to the X-ray emission at these epochs. Instead, it supports a leptonic origin for the X-ray emission in BL Lac.

Unified Astronomy Thesaurus concepts: Relativistic jets (1390); X-ray active galactic nuclei (2035); Active galactic nuclei (16); Blazars (164); Spectropolarimetry (1973)

1. Introduction

Observations of astrophysical jets from supermassive black holes offer unique opportunities to study energetic multiwave band emission processes in the universe (see, e.g., Blandford et al. 2019). Blazars are a subclass of active galactic nuclei (AGNs) whose jets are aligned within a few degrees of the line of sight. They are often characterized by the superluminal motion of bright knots in their jets, and their emission, which is relativistically Doppler boosted, exhibits extreme variability

[†] While the AAS journals adhere to and respect UN resolutions regarding the designations of territories (available at http://www.un.org/press/en), it is our policy to use the affiliations provided by our authors on published articles.

across the electromagnetic spectrum (e.g., Hovatta & Lindfors 2019). Their radio and optical emission is significantly linearly polarized (e.g., Agudo et al. 2018a; Blinov et al. 2021), which is attributed to synchrotron radiation from relativistic electrons in the jet. The origin of the broad keV-to-TeV emission component is a matter of current debate. Most studies interpret the high-energy photons as the result of Compton scattering. The seed photons could originate from either the jet's synchrotron radiation (synchrotron self-Compton; SSC) or from external radiation fields (external Compton; EC). This scenario has been supported by spectral energy distribution (SED, e.g., Abdo et al. 2011) modeling, energetic considerations (Zdziarski & Bottcher 2015; Liodakis & Petropoulou 2020), observations of flux variations that are correlated across the wave bands (e.g., Agudo et al. 2011a, 2011b; Liodakis et al. 2018, 2019b), and low or even undetected radio/optical circular polarization (Wardle et al. 1998; Liodakis et al. 2022a). However, scenarios invoking proton-initiated emission (synchrotron radiation by relativistic protons, and/or emission processes associated with cascades of leptons produced by photohadronic processes, e.g., IceCube Collaboration et al. 2018) have not been definitively excluded. Typically, leptonic models have been more successful in modeling low synchrotron peaked blazars (LBL, $\nu_{\rm syn} < 10^{14}$ Hz), while hadronic models are often favored for high-synchrotron-peak sources ($\nu_{\rm syn} > 10^{15}$ Hz, e.g., Böttcher et al. 2013; Cerrutti et al. 2015, 2017).

Measurements of X-ray polarization can be used to test high-energy emission processes and particle acceleration in jets (e.g., Zhang & Bottcher 2013; Tavecchio et al. 2018; Liodakis et al. 2019a). Starting in 2022 January, the Imaging X-ray Polarimetry Explorer (IXPE; Weisskopf et al. 2010, 2016, 2022) has been carrying out such measurements. Detection by IXPE of high-synchrotron-peak sources like Mrk 501 and Mrk 421 (Di Gesu et al. 2022; Liodakis et al. 2022b) has revealed stronger polarization at X-rays than at longer wavelengths. This is consistent with emission by high-energy electrons that are accelerated at a shock front with partially ordered magnetic fields, after which they are advected to regions with more turbulent fields.

Here we report the first X-ray polarimetric observations of an LBL blazar, the eponymous source BL Lacertae (BL Lac, $z = 0.0686$, Vermeulen et al. 1995). The X-ray emission of BL Lac is highly variable, with an average flux of $F_{2-10\,\rm keV} \sim 1 \times 10^{-11}$ erg cm^{-2} s^{-1} (e.g., Wehrle et al. 2016; Giommi et al. 2021; Middei et al. 2022; Sahakyan & Giommi 2022). Moreover, BL Lac is a very high energy emitting source as it is the 14th brightest AGN at γ-ray energies listed in the Fermi 4LAC catalog (Ajello et al. 2020) and among the few LBL sources detected in TeV γ-rays showing fast, even down to ∼hourly timescales, flux variability (Albert et al. 2007; Arlen et al. 2013). Moreover, BL Lac has been the focus of a large number of multiwavelength and polarization studies (e.g., Raiteri et al. 2013; Blinov et al. 2015, 2018; Weaver et al. 2020; Casadio et al. 2021).

This Letter is organized as follows. We describe the IXPE observations and X-ray data processing and analysis in Section 2 and our contemporaneous observing campaign atoptical circular polarization, infrared, and optical wavelengths in Section 3. In Section 4 we test the interplay among the radio/optical and X-ray bands and we discuss and interpret our results in Section 5. A standard ΛCDM cosmology with $H_0 = 70$ km s^{-1} Mpc^{-1}, $\Omega_{\rm m} = 0.27$, and $\Omega_\lambda = 0.73$ is adopted throughout this work. Errors quoted in text and in plots correspond to 1σ uncertainties ($\Delta\chi^2 = 1$ for 1 parameter of interest). All upper limits related to IXPE observations are quoted at 99% confidence, corresponding to $\Delta\chi^2 = 6.635$ for 1 parameter of interest.

Table 1
Log of X-Ray Observations Related to the IXPE Pointings of BL Lac

Observatory	ObsID	Observation date (yyyy-mm-dd)	Net exposure (ks)
IXPE	01006301	2022/05/06-14	∼390
NuSTAR	60701036002	2022/5/6	∼22
XMM-Newton	0902111001	2022/5/15	∼7
IXPE	01006701	2022/7/7–9	∼116
XMM-Newton	0902111301	2022/7/8–9	∼15

Note. The log of the Swift exposures and the corresponding derived quantities are reported in Appendix B.

2. X-Ray Spectra and Polarization Observations

BL Lac was observed with the three detector units (DUs) of IXPE during 2022 May 6–14 for a net exposure of 390 ks. The second observation was performed 2022 July 9–11 for a net exposure of ∼116 ks. Quasi-simultaneously with the first IXPE observation, BL Lac was observed by the Nuclear Spectroscopic Telescope Array (NuSTAR; Harrison et al. 2013), with a ∼25 ks exposure, and with the EPIC-pn (Struder et al. 2001) camera on board XMM-Newton (Jansen et al. 2001). In addition, another XMM-Newton observation was taken simultaneously with the second IXPE observation of BL Lac. In Appendix A.3, we report the details on the data reduction of the IXPE, XMM-Newton, and NuSTAR data. The X-Ray Telescope (XRT; Burrows et al. 2005) on the Neil Gehrels Swift Observatory (Swift) monitored the blazar from 2022 May until July. The log of the exposures is provided in Table 1 and details on data reduction and the results of these observations are provided in Appendix A.3.

2.1. X-Ray Spectral Analysis

We combine the IXPE Stokes I (i.e., total flux density), XMM-Newton, and (only for the first exposure) NuSTAR data to determine the X-ray spectrum in the 0.5–79 keV energy range. We first attempt to fit the data with a simple model of a single power-law continuum with photoelectric absorption exceeding that from gas in our Galaxy. In fact, various studies (e.g., Bania et al. 1991; Madejski et al. 1999) have reported on the presence of neutral absorption in this source, invoking the presence of molecular clouds along the line of sight to BL Lac. We thus have fit the column density requiring a consistent value for both observations 1 and 2. Then, a constant was used to account for the cross calibration among instruments and any variability due to the nonstrict simultaneity of the exposures. To fit the data, we fit the photon index and the normalization of the power law separately for each of the two data sets, i.e., observation 1 (IXPE, XMM-Newton, and NuSTAR) and observation 2 (IXPE and XMM-Newton). These steps led to a good fit with the χ^2 statistic $\chi^2/{\rm dof} = 1234/1112$. The column density derived exceeds the Galactic value as expected. Both XMM-Newton observations show bump-like residuals around 0.7 keV, which we infer as being due to an additional spectral component. We speculate that it represents emission

from hot diffuse plasma, which we include as an *apec* model in XSPEC. We fit the temperature and the normalization of this *apec* component while requiring its temperature and normalization to be consistent between the two data sets. This step led us to a satisfactory spectral fit (χ^2/dof= 1169/1110). We attempted to replace the apec component with a single Gaussian centered at 0.7 keV; however, this returned a worse fit with $\Delta\chi^2 = +31$ for the same number of degrees of freedom. Finally, the present data set does not support the presence of a synchrotron component at soft X-ray energies, which would be the tail of the low energy hump of the SED. Replacing the *apec* model with such a steep power-law component degrades the quality of the fit to the data ($\Delta\chi^2 = +52$ with two additional free parameters).

The cross-normalization constants between IXPE and XMM-Newton were consistent with unity within ∼10%. The difference between the IXPE and NuSTAR flux normalizations was ∼30%, although this could be mainly ascribed to the flux level of BL Lac being higher during the NuSTAR pointing than the average during the IXPE exposure.

Based on our model fits, the X-ray spectrum of BL Lac beyond ∼2 keV was characterized by a power law with photon index $\Gamma = 1.74 \pm 0.01$ and 1.87 ± 0.06 for observations 1 and 2, respectively. The source was in a higher flux level during the later epoch. The absorbing column density is found to be $N_{\rm H} = 2.60 \pm 0.05 \times 10^{21}$ cm^{-2} and this value is in perfect agreement with the extensive analysis performed by Weaver et al. (2020). At low energies, below the IXPE bandpass, the spectra are consistent with emission from hot gas ($kT = 0.38 \pm 0.04$ keV). However, the physical origin of such an additional soft component is unknown and requires additional observations to determine.

2.2. Spectropolarimetric X-Ray Analysis

We searched for X-ray polarization from BL Lac by performing a spectropolarimetric fit of the *I*, *Q*, and *U* Stokes spectra over the two IXPE exposures. To better constrain the spectral shape of BL Lac we performed the spectropolarimetric analysis also including the XMM-Newton and NuSTAR data. Similarly to the fit to the *I* Stokes spectra, we fitted simultaneously the Galactic column density and the *apec* component, while the photon index and the normalization of the power law were computed for each observation. We then accounted for the polarimetric information encoded in the *Q* and *U* Stokes parameters multiplying the power law with *polconst*, i.e., an XSPEC model that assumes the polarization signal to be constant across the IXPE energy range. Thus, the final model consists of *tbabs* × *const* × (*apec* + *polconst* × *powerlaw*), in XSPEC notation. The constant accounts for the intercalibration among the different detector units. We first fit separately the two IXPE observations with the polarization degree and angle free to vary between exposures. This procedure leads to a best fit of $\chi^2 = 1469$ for 1388 dof, and provides two upper limits for the polarization degree: $\Pi_X = < 14.2\%$ and $\Pi_X < 12.6\%$ (at 99% confidence level) for observations 1 and 2, respectively. In Figure 1 we display the fit to the two IXPE exposures and the corresponding confidence regions. In Table 2 we report the best-fit values corresponding to the analysis of the IXPE observations. Then we tested a scenario where both Π_X and ψ_X remained unchanged between observations. Although blazars typically vary on shorter timescales than 2 months, this test is motivated by the fact that the polarization angle in the millimeter/radio energy range ψ_R (see Section 3), i.e., the seed photons in case of synchrotron self-Compton emission, is consistent within uncertainties between the two observations (see Appendix A). Moreover, as found for hadronic models including polarization, X-ray polarization is expected to be less variable than at optical wavelengths (Zhang et al. 2016). This simple test yields a compatible fit (χ^2/dof = 1473/1390), with the spectral parameters being consistent with those quoted in Table 2. Also in this case, we obtain only an upper limit to the polarization degree, $\Pi_X < 9.6\%$, and the polarization angle is unconstrained. We subsequently set the polarization degree to be the same between the observations, but allow the polarization angle to vary. This attempt, which yields only a compatible fit statistic, gives $\Pi_X < 11.1\%$ with no information on the polarization angle. We also tested the opposite scenario in which the polarization angle is constant between the two IXPE exposures and Π_X varies. Such a test, to which corresponds an equivalent fit statistic, led us to an unconstrained X-ray polarization angle and upper limits for the polarization degrees of $\Pi_X < 14.2\%$ and $\Pi_X < 11.7\%$ for the two observations.

3. Multiwavelength Observations

During the IXPE observations, a number of telescopes provided multiwavelength polarization coverage: the Atacama Large Millimeter/submillimeter Array (ALMA), AZT-8 (Crimean Astrophysical Observatory, 70 cm diameter), Calar Alto (Spain, 2.2 m), Haleakala T60 (Hawaii, USA), Institut de Radioastronomie Millimétrique (IRAM, 30 m), St. Petersburg University LX-200 (40 cm), Kanata telescope (Japan), Nordic Optical Telescope (NOT, La Palma, Spain, 2.56 m), Palomar Hale telescope (California, USA, 5 m), Boston University Perkins Telescope (1.8 m, Flagstaff, Arizona, USA), the Sierra Nevada Observatory (1.5 and 0.9 m telescopes, Spain), the Skinakas observatory (Crete, Greece, 1.3 m telescope), and the Submillimeter Array (SMA). The observations and data reduction are described in Appendix A. Figures 2, 3, and 4 display the millimiter, optical, and infrared polarized light curves of BL Lac during the IXPE observing windows. During the second IXPE observation, we were unable to obtain infrared polarization data. During both IXPE observations, we find significant variability in polarization degree and angle at millimeter to optical wavelengths.

For IXPE observation 1, the ALMA observations on May 7 yield a median radio polarization degree $\Pi_R = 3.95\% \pm 0.3\%$ at 343 GHz along position angle $\psi = 23° \pm 2°$, and, on May 9, $\Pi_R = 3.6\% \pm 0.3\%$ along $\psi_R = 33° \pm 1°$. The two values of Π_R are consistent between scans within the uncertainties. This is also true for ψ_R during the May 7 observation. However, on May 9 we see a change in ψ_R from the first to the final scan from 19° to 46°. The median uncertainty of each measurement is ±1°. The IRAM 30 m measurements are the same within the uncertainties, which suggests that there is no significant variability. The median value of Π_R at 86 GHz is 4% with a median uncertainty of 0.4% along a median position angle $\psi_R = 30° \pm 3°$. Similarly, at 228.93 GHz, the median $\Pi_R = 4.8\% \pm 1.2\%$ along median $\psi = 35° \pm 7°$. No circular polarization was detected in any of the observations, with a 95% confidence-interval upper limit of <0.44% and <0.86% for 86 GHz and 228.93 GHz, respectively. We find the optical polarization degree Π_O to vary from 1.6% to 13.7%, with a median of 6.8%. At the same time ψ_O varies from 2° to 172° with a median of 107°, almost perpendicular to the jet axis on

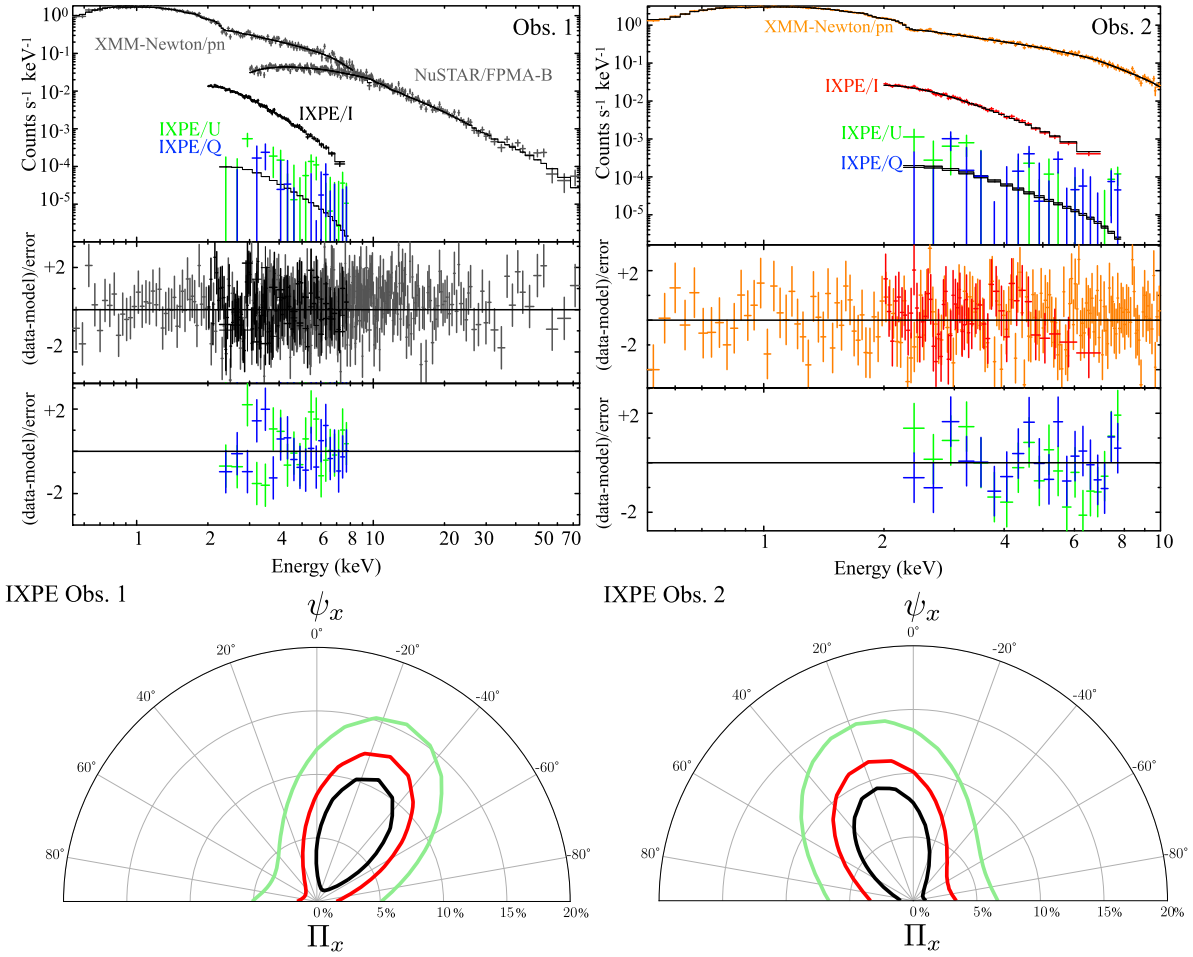

Figure 1. Top panels: best fit to the May X-ray data set (on the left) and the IXPE-XMM-Newton data taken during 2022 July (right plots). In the middle and bottom subpanels, we report the residuals to the *I*, *U*, and *Q* spectra, respectively. Bottom plots: confidence regions of the model fits for the polarization angle and degree for the two observations.

Table 2
Best-fit Parameters for the Two IXPE Observations

Model	Component	Observation 1	Observation 2
polconst	Π_X	<14.2%	<12.6%
	ψ_X	…	…
tbabs	$N_{\rm H}$†	2.60 ± 0.05	
apec	kT (keV)†	0.38 ± 0.04	
	Normalization	3.1 ± 0.1	
powerlaw	Γ	1.74 ± 0.01	1.87 ± 0.06
	Norm	2.74 ± 0.05	5.5 ± 0.1
$F_{2-8\ \rm keV}$		$0.96 \pm 0.03(0.05)$	$1.56 \pm 0.06(0.09)$

Note. The power-law normalization is in units of $\times 10^{-3}$ photons keV^{-1} cm^{-2} s^{-1}, the apec component has a normalization of $\times 10^{-4}$, and fluxes are $\times 10^{-11}$ erg cm^{-2} s^{-1}. Errors accounting for the polarimetric information refer to a 99% confidence interval for one parameter of interest.

the plane of the sky ($10^\circ \pm 2$, Weaver et al. 2022). In the infrared, $\Pi_{\rm IR}$ varies from 0.9% to 8.4% with a median of 3.9%. Note that, although the host galaxy has a negligible contribution to the total emission in the optical during the IXPE observation, it is likely that the contribution is much stronger in the infrared. Hence, the $\Pi_{\rm IR}$ measurements should be treated as lower limits to the intrinsic polarization degree. The value of $\psi_{\rm IR}$ varies from 9° to 158° with a median of ∼83°.

During the July IXPE observation, the polarization degree detected by the IRAM 30 m Telescope decreases at 86GHz from 8.5% to 2.2% with a constant median ψ_R of ∼15°; see Figure 2. The SMA observation at 225 GHz yields $\Pi_R = 8.8 \pm 1\%$ along ψ_R of $19^\circ \pm 2^\circ$. The polarization at 228 GHz is consistent within uncertainties at about $\Pi_R = 6\%$ along $\psi_R \approx 20^\circ$. At the same time the optical polarization varies from 7% to 23% with a median of $\Pi_O = 14.2\%$, with ψ_O between 26° and 59° with a median of $\psi_O = 42^\circ$. A summary of these observations and their polarimetric information is provided in Appendix A.

4. Connections of the X-Ray Polarization with the Radio and Optical Bands

In both leptonic and hadronic models, the X-ray polarimetric properties are tightly related to those at the millimeter-radio and optical bands, respectively. Motivated by that close connection, we performed additional tests, fixing ψ_X to the corresponding values of ψ_R and ψ_O and computing Π_X for the IXPE observations. In an SSC scenario, we expect the polarization angle to be similar to the one of the millimeter-radio seed photons. On the other hand, in hadronic scenarios, the optical polarization degree is expected to be similar to Π_X. Motivated by these expectations, we proceed to restrict the polarization parameters. We therefore first restrict ψ_X to the value of the

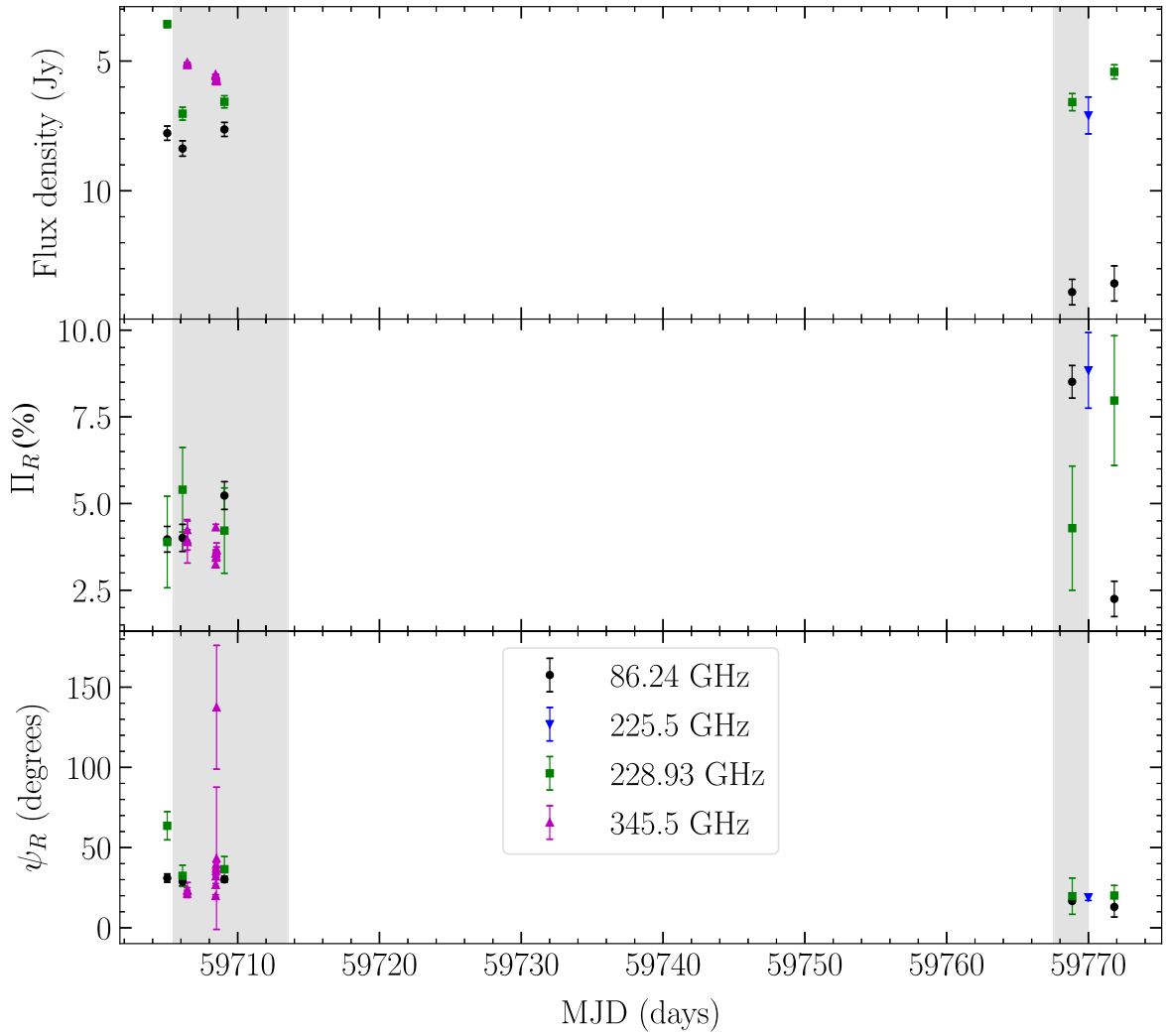

Figure 2. Radio polarization vs. time for BL Lac object. Top: flux density; middle: polarization degree; bottom: polarization angle. The gray shaded areas demark the duration of IXPE observations 1 and 2.

millimeter-radio observations. This seems to improve the $\Pi_X <$ upper limits when fitting the observations separately ($\Pi_X < 6.2\%$ and $\Pi_X < 12.9\%$ for observations 1 and 2, respectively). We repeat the exercise, but this time we restrict ψ_X to the average value of the optical observations. We see a marginal improvement for the second observation with $\Pi_X < 14.2\%$ and $\Pi_X < 11.9\%$ for observations 1 and 2, respectively. Since ψ_O change by more than 70° from the first to the second IXPE observation we do not attempt a joined fit. The derived upper limits from these tests are also summarized in Table 3. Although improved upper limits as low as <6.2% can be obtained for the first IXPE observation, none of these attempts significantly enhanced or degraded the fit to the data presented in Section 2.2. In Table 3 we report the corresponding upper limits from our tests.

5. Discussion and Conclusions

We have presented the first X-ray polarization observations of an LBL blazar, BL Lac. The analysis of the IXPE data only provides upper limits (corresponding to the 99% confidence level) to the polarization degree: $\Pi_X < 14.2\%$ and $\Pi_X < 12.6\%$ for the first and second exposure, respectively. As a consequence, the polarization angle ψ_X is unconstrained for both of the observations. The upper limit to Π_X can be decreased to as low as <6% by making assumptions for the Π_X and ψ_X only for the first IXPE observation. The upper limits can then be compared with the polarization at longer wavelengths (whose properties are quoted in Tables 4 and 5 in Appendix A). In the optical, we measure a median $\Pi_O = 6.8\%$ at a median angle of $\psi_O = 107°$ for the May observation and medians $\Pi_O = 14.2\%$ and $\psi_O = 42°$ for the July observation. We find evidence of significant millimeter-radio to optical polarization variability during both IXPE observations. Moreover, the variability in the polarization angle is stronger in the optical. Changes in the ψ due to perhaps turbulence or multiple emission regions would reduce the observed polarization degree by $1/\sqrt{N}$, where N is the number of emission regions or turbulent cells (Marscher 2014). Considering the IXPE upper limits derived over the observing period, the median Π_O during the May observation was a factor of ∼2.5 lower, whereas for the July observation Π_O was higher than the Π_X limit.

A strong synchrotron X-ray component from ultra-high-energy electrons can also occur in BL Lac, but in this case the X-ray spectrum would be much steeper than that of our model fits (Marscher et al. 2008). In a leptonic scenario, under which X-ray and γ-ray emission arises from Compton scattering, the

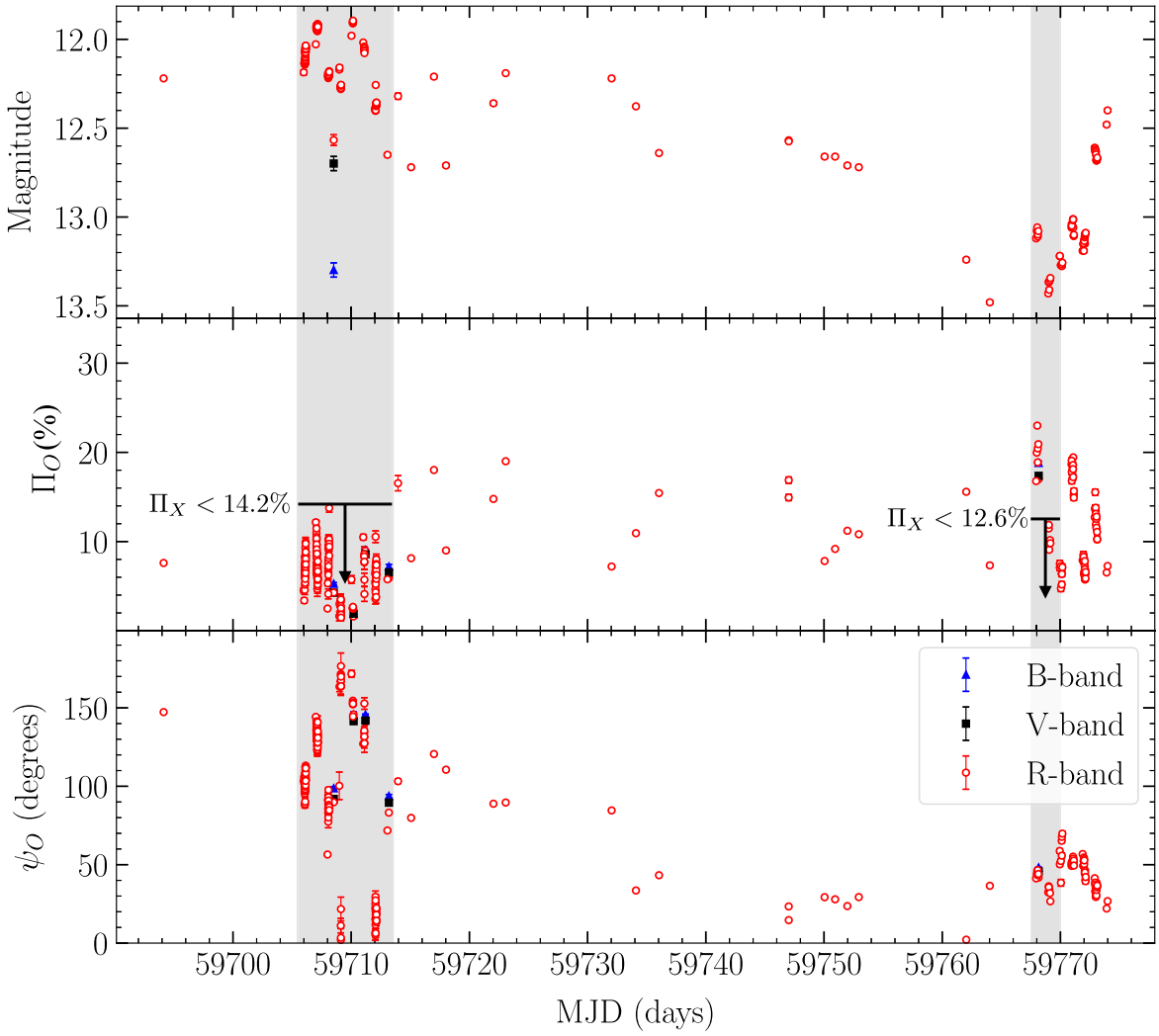

Figure 3. Optical polarization time variations for BL Lac object. Top: magnitude; middle: polarization degree; bottom: polarization angle. The gray shaded areas demark the duration of the IXPE observations. The IXPE upper limits obtained in the two observations are also reported.

X-ray polarization degree is expected to be substantially lower than that of the seed photons (Bonometto & Saggion 1973; Nagirner & Poutanen 1993; Poutanen 1994; Liodakis et al. 2019a; Peirson & Romani 2019). In the case of EC scattering, depending on the scattering geometry and isotropy of the seed photon field, the outgoing radiation could be either unpolarized or polarized. However, based on previous SED modeling (Böttcher & Bloom 2000; Böttcher et al. 2013; MAGIC Collaboration et al. 2019; Morris et al. 2019; Sahakyan & Giommi 2022) we expect SSC emission to be dominated over the EC one in the IXPE energy band. In an SSC model, the seed photons are expected to come from millimeter-radio synchrotron radiation. The millimeter-radio observations give $\Pi_R \sim 4\%$ for the first observation and $\Pi_R \sim 6\%$ for the second. This would suggest an expected Π_X of $<3\%$ (Peirson & Romani 2019). Therefore, our upper limits for any X-ray polarization signal are consistent with a leptonic scenario. On the other hand, in the case of hadronic processes, X-ray polarization should be less variable, or even stable, compared to the optical, with negligible depolarization (Zhang et al. 2016). The contribution from synchrotron radiation by protons and secondary particles from collisions involving hadrons is expected to yield a similar, or higher (in the case of a pure proton-synchrotron model) value of Π_X compared to optical wavelengths (Zhang & Bottcher 2013; Paliya et al. 2018; Zhang et al. 2019). Alternative emission models involving scattering from relativistic cold electrons are also expected to produce much higher Π_X than Π_O (Begelman et al. 1987). During both IXPE observations, Π_O exceeded the 99% upper limits of Π_X on several occasions. Even considering the median Π_O estimates during the IXPE observations, the optical still exceeds the X-ray upper limit for the July observation. This difference between the optical and X-ray polarization degrees is in strong tension with the relativistic cold electron scattering model as well as a pure proton-synchrotron model. Although we cannot definitively exclude contribution from hadronic processes to the overall emission, the multiwavelength polarization observations provide evidence against the hadronic interpretation. Instead, our findings favor leptonic emission, and particularly Compton scattering as the dominant mechanism for the X-ray emission in BL Lac.

We thank the anonymous referee for their bright comments. The Imaging X-ray Polarimetry Explorer (IXPE) is a joint US and Italian mission. The US contribution is supported by the National Aeronautics and Space Administration (NASA) and led

and managed by its Marshall Space Flight Center (MSFC), with industry partner Ball Aerospace (contract NNM15AA18C). The Italian contribution is supported by the Italian Space Agency (Agenzia Spaziale Italiana, ASI) through contract ASI-OHBI-2017-12-I.0, agreements ASI-INAF-2017-12-H0 and ASI-INFN-2017.13-H0, and its Space Science Data Center (SSDC), and by the Istituto Nazionale di Astrofisica (INAF) and the Istituto Nazionale di Fisica Nucleare (INFN) in Italy. This research used data products provided by the IXPE Team (MSFC, SSDC, INAF, and INFN) and distributed with additional software tools by the High-Energy Astrophysics Science Archive Research Center (HEASARC), at NASA Goddard Space Flight Center (GSFC). We acknowledge financial support from ASI-INAF agreement n. 2022-14-HH.0. The research at Boston University was supported in part by National Science Foundation grant AST-2108622 and NASA Swift Guest Investigator grant 80NSSC22K0537. This research has made use of data from the RoboPol program, a collaboration between Caltech, the University of Crete, IA-FORTH, IUCAA, the MPIfR, and the Nicolaus Copernicus University, which was conducted at Skinakas Observatory in Crete, Greece. The IAA-CSIC coauthors acknowledge financial support from the Spanish "Ministerio de Ciencia e Innovacion" (MCINN) through the "Center of Excellence Severo Ochoa" award for the Instituto de Astrofísica de Andalucía-CSIC (SEV-2017-0709). Acquisition and reduction of the POLAMI, TOP-MAPCAR, and OSN data was supported in part by MICINN through grants AYA2016-80889-P and PID2019-107847RB-C44. The POLAMI observations were carried out at the IRAM 30 m Telescope. IRAM is supported by INSU/CNRS (France), MPG (Germany), and IGN (Spain). This Letter makes use of the following ALMA director's discretionary time data under proposal ESO#2021.A.00016.T. ALMA is a partnership of ESO (representing its member states), NSF (USA), and NINS (Japan), together with NRC (Canada), MOST, and ASIAA (Taiwan), and KASI (Republic of Korea), in cooperation with the Republic of Chile. The Joint ALMA Observatory is operated by ESO, AUI/NRAO, and NAOJ. Some of the data reported here are based on observations obtained at the Hale Telescope, Palomar Observatory as part of a continuing collaboration between the California Institute of Technology, NASA/JPL, Yale University, and the National Astronomical Observatories of China. This research made use of Photutils, an Astropy package for detection and photometry of astronomical sources (Bradley et al. 2019). G.V.P. acknowledges support by NASA through the NASA Hubble Fellowship grant #HST-HF2-51444.001-A awarded by the Space Telescope Science Institute, which is operated by the Association of Universities for Research in Astronomy, Inc., under NASA contract NAS5-26555. The data in this study include observations made with the Nordic Optical Telescope, owned in collaboration by the University of Turku and Aarhus University, and operated jointly by Aarhus University, the University of Turku, and the University of Oslo, representing Denmark, Finland, and Norway, the University of Iceland and Stockholm University at the Observatorio del Roque de los Muchachos, La Palma, Spain, of the Instituto de Astrofisica de Canarias. The data presented here were obtained in part with ALFOSC, which is provided by the Instituto de Astrofísica de Andalucía (IAA) under a joint agreement with the University of Copenhagen and NOT. E.L. was supported by Academy of Finland projects 317636 and 320045. Part of the French contribution is supported by the Scientific Research National Center (CNRS) and the French Spatial Agency (CNES). Some of the data are based on observations collected at the Observatorio de Sierra Nevada, owned and operated by the Instituto de Astrofísica de Andalucía (IAA-CSIC). Further data are based on observations collected at the Centro Astronómico Hispano-Alemán (CAHA), operated jointly by Junta de Andalucía and Consejo Superior de Investigaciones Científicas (IAA-CSIC). D.B., S.K., R.S., and N. M. acknowledge support from the European Research Council (ERC) under the European Unions Horizon 2020 research and innovation program under grant agreement No. 771282. C.C. acknowledges support by the European Research Council (ERC) under the HORIZON ERC Grants 2021 program under grant agreement No. 101040021. The Dipol-2 polarimeter was built in cooperation by the University of Turku, Finland, and the Leibniz Institut für Sonnenphysik, Germany, with support from the Leibniz Association grant SAW-2011-KIS-7. We are grateful to the Institute for Astronomy, University of Hawaii, for the allocated observing time. A.H. acknowledges The National Radio Astronomy Observatory is a facility of the National Science Foundation operated under cooperative agreement by Associated Universities, Inc. This work was supported by JST, the establishment of university fellowships toward the creation of science technology innovation; grant No. JPMJFS2129. This work was supported by Japan Society for the Promotion of Science (JSPS) KAKENHI grant Nos. JP21H01137. This work was also partially supported by Optical and Near-Infrared Astronomy Inter-University Cooperation Program from the Ministry of Education, Culture, Sports, Science and Technology (MEXT) of Japan. We are grateful to the observation and operating members of Kanata Telescope. The Submillimeter Array is a joint project between the Smithsonian Astrophysical Observatory and the Academia Sinica Institute of Astronomy and Astrophysics and is funded by the Smithsonian Institution and the Academia Sinica. Maunakea, the location of the SMA, is a culturally important site for the indigenous Hawaiian people; we are privileged to study the cosmos from its summit.

Facilities: ALMA, CAO:2.2m, CrAO:0.7m, Hale, IRAM:30m, IXPE, Kanata, LX-200, NOT, NuSTAR, OSN:0.9m, OSN:1.5m, Perkins, Skinakas:1.3m, SMA, Swift, TU:0.6m, XMM-Newton.

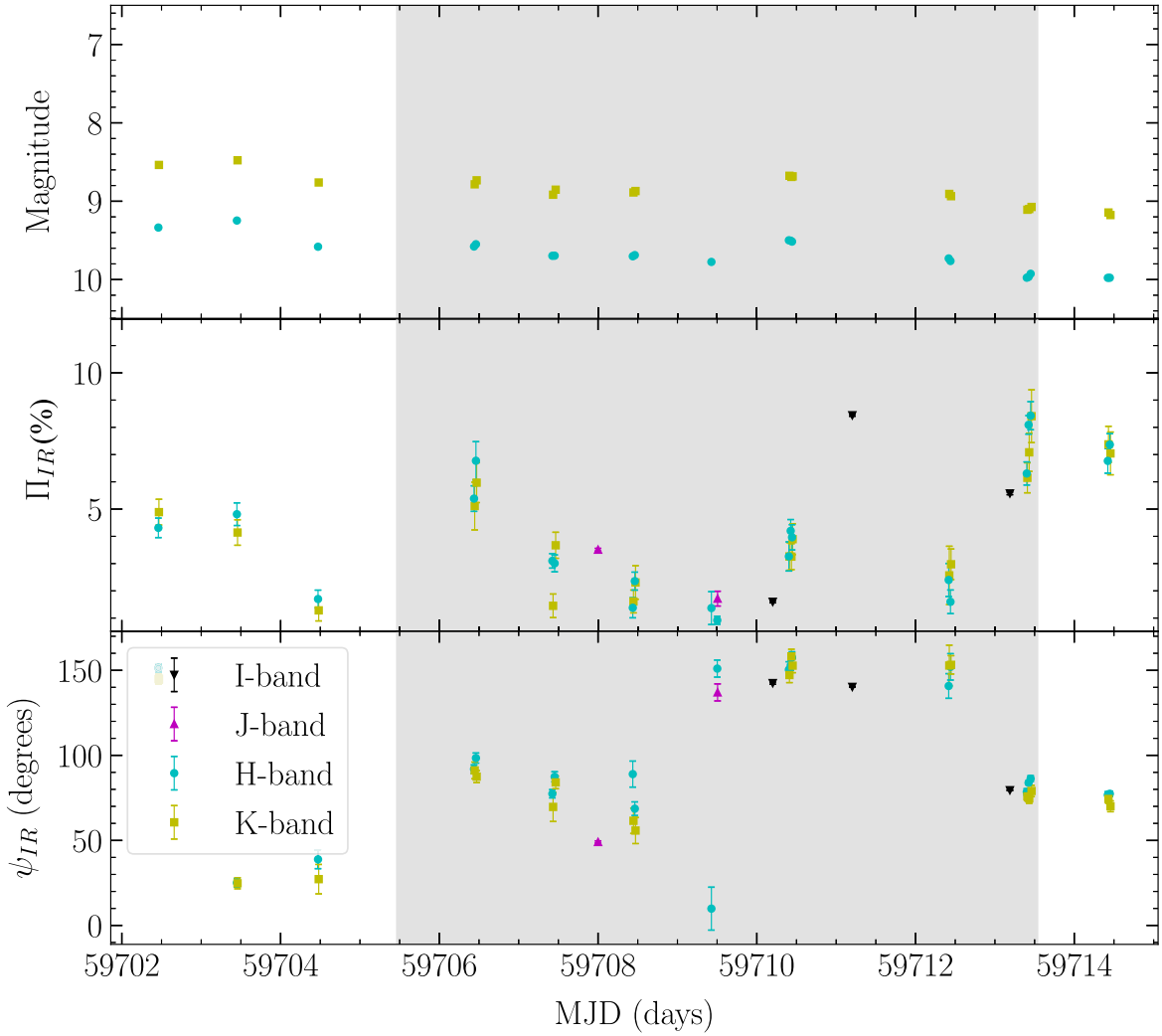

Figure 4. Infrared polarization vs. time for BL Lac object. Top: magnitude; middle: polarization degree; bottom: polarization angle. The gray shaded area demarks the duration of IXPE observation 1.

Table 3
The Upper Limits for the X-Ray Polarization Degree Π_X Derived Assuming the X-Ray Polarization Angle to Be the Same as the Average Values for ψ_O and ψ_R

Optical Angle	$\Pi_X^{\rm Obs1}$	$\Pi_X^{\rm Obs2}$
$\psi_O^{\rm Obs1}$=112°	<14.2%	
$\psi_O^{\rm Obs2}$=38°		<11.9%
Radio angle		
$\psi_R^{\rm Obs1}$=30°	< 6.2%	
$\psi_R^{\rm Obs2}$=18°		<12.9%

Note. Upper limits were computed for both the IXPE observations.

Appendix A
Multiwavelength Observations

A.1. Millimeter-radio Observations

Radio polarization observations were obtained at millimeter and submillimeter wavelengths using ALMA, the Institut de Radioastronomie Millimétrique 30 m Telescope (IRAM 30m), and SMA. The ALMA observations were obtained in band 7 (mean wavelength of 0.87 mm, frequency 345 GHz) on 2022 May 7 and 9. The ALMA observations were reduced using the AMAPOLA[77] polarization pipeline, which is used to estimate polarization properties from short monitoring observations of ALMA grid sources for calibrator selection. It aims to determine the D-terms for instrumental calibration from short scans of different sources with sufficient signal to noise ratio (S/N) and employs an antenna-based database for a priori values assuming stability. Thus the method is applicable for observations when less than 60 degrees of field rotation (parallactic angle) is achieved on the polarization calibrator. The standard reduction procedure assumes a larger parallactic angle coverage for the determination of the D-terms on the polarization calibrator, which are then transferred instantaneously for the calibration of the target.[78,79] The SMA observation was obtained within the SMAPOL monitoring program on 2022 July 10 at 1.3 mm corresponding to 225.538 GHz. The IRAM 30 m observations were performed

[77] http://www.alma.cl/~skameno/AMAPOLA/
[78] http://www.alma.cl/~skameno/POLBEAM/ShortCalibrationSchemeTests20170321.pdf, http://www.alma.cl/~skameno/POL/ShortPOL/ShortPolCal20170830.pdf
[79] http://www.alma.cl/~skameno/POL/ShortPOL/ShortPolCal20170830.pdf

on 2022 May 5, 7, and 10, and again on 2022 July 8 and 11 at 3.5 mm (86.24 GHz) and 1.3 mm (228.93 GHz) as part of the IRAM's Polarimetric Monitoring of AGN at Millimeter Wavelengths (POLAMI) Large Project[80] (Agudo et al. 2018a, 2018b; Thum et al. 2018). In Figure 2 we show the millimeter-radio polarization light curve.

A.2. Optical and Infrared Observations

During IXPE observation 1, BL Lac was observed in optical polarization by the AZT-8 telescope (2022 May 6–11), the Calar Alto observatory (2022 May 7, 9, 11, and July 7–9), the Haleakala observatory T60 telescope (2022 May 9), Kanata telescope (2022 May 9), the Nordic Optical Telescope (NOT; 2022 May 11, 12, and 14, and 2022 July 7), Palomar observatory (Hale, 2022 May 10), the Perkins observatory (2022 May 3–5, 7–11, 13–15), the St. Petersburg University LX-200 telescope (2022 May 6, 9, 14), the Sierra Nevada observatory (T90 and T150, 2022 May 7–13, and July 9), and the Skinakas observatory (RoboPol, 2022 May 14, 16, and July 7, 9). The Calar Alto Observatory observations used the 2.2 m telescope and the imaging polarimetric mode of the Calar Alto Faint Object Spectrograph. Observations were obtained in the R_c filter and reduced using both unpolarized and polarized standards stars and following standard analysis procedures. Similar procedures and the same filters were used for the T90 and T150 telescope observations at the Sierra Nevada Observatory. We performed R-band polarimetric observations with the Hiroshima Optical and Near-InfraRed camera (HONIR, Akitaya et al. 2014) installed on the Kanata telescope. The polarization degree, polarization angle, and corresponding errors were estimated from Stokes parameters obtained from four exposures at positions 0°, 45°, 22.°5, and 67.°5 of the half-wave plate for each observation (Kawabata et al. 1999). Offset angle and wire grid depolarization were corrected using highly polarized standard stars (BD+64d106, BD+59d389). The instrumental polarization was determined with the help of unpolarized standard stars (HD 14069) to be $<0.2\%$. We also obtained linear polarimetric observations with the Alhambra Faint Object Spectrograph and Camera (ALFOSC) in B, V, R, I bands of the BL Lac object, along with polarized and unpolarized standard stars during each of the observing nights for instrumental calibration. The data were reduced following standard photometric procedures included in the Tuorla Observatory's data reduction pipeline, described in detail in Hovatta et al. (2016) and Nilsson et al. (2018). The T60 telescope uses the "double-image" CCD polarimeter Dipol-2 (Piirola et al. 2014). Dipol-2 is capable of simultaneously observing in B, V, and R filters (Piirola 1973; Berdyugin et al. 2018, 2019; Piirola et al. 2021). The instrumental polarization and zero-point of the polarization angle were determined by observing polarized and unpolarized standard stars, and the measurements are combined using the "2× sigma-weighting algorithm." The standard error of the weighted means of the normalized Stokes parameters are then propagated to obtain the final uncertainty of the polarization degree and angle (Kosenkov et al. 2017; Piirola et al. 2021). The Skinakas observatory observations used the RoboPol instrument mounted in the 1.3 m telescope (Ramaprakash et al. 2019). RoboPol is a novel four-channel polarimeter that simultaneously measures the normalized Stokes q and u parameters with a single exposure and no moving parts. The data reduction and analysis pipeline is described in detail in Panopoulou et al. (2015) and Blinov et al. (2021). The 40 cm LX-200 and 70 cm AZT-8 telescopes are equipped with nearly identical imaging photopolarimeters based on an ST-7 camera, using and swapping two Savart plates oriented 45° with respect to each other. The observations were performed in the R-band and the data were background, bias, and flat-field corrected, as well as instrumental- and interstellar-polarization calibrated with the use of standard stars.

In addition to the optical measurements, we obtained observations in the J, H, and K infrared bands using the 200 inch Palomar Hale telescope, the Kanata telescope, and the WIRC+Pol instrument (Tinyanont et al. 2019b). The Hale telescope observations were performed in the J and H bands using a polarized grating to simultaneously measure four linearly polarized components, while a half-wave plate improved polarimetric sensitivity by beam swapping (Tinyanont et al. 2019a; Millar-Blanchaer et al. 2021). The data were reduced using the WIRC+Pol Data Reduction Pipeline software[81], described in detail in Tinyanont et al. (2019b) and Masiero et al. (2022). The Kanata observation was performed in the J band simultaneously to the R band observation (see above). Data from the Perkins Telescope were obtained in the H and K bands, using the IR camera MIMIR.[82] One measurement consists of six dithering exposures of 3 s each at 16 positions of a half-wave plate, rotated in steps of 22.°5 from 0 to 360°. The camera and data reduction are described in detail in Clemens et al. (2012).

A.3. X-Ray Observations

We here present the data reduction of the different data set studied in Section 2 and obtained using IXPE, XMM-Newton and NuSTAR. In Table 1, we summarize their corresponding information.

For both IXPE observations, the cleaned event files and the associated science products were obtained using a dedicated pipeline relying on the *Ftools* software package and adopting the latest calibration data files from IXPE (CALDB 20211118). The source regions for each of the three DUs were then selected via an iterative process aimed at maximizing the S/N in the IXPE operating energy range of 2–8 keV. In particular, we used circular regions with radius 47″ for all three DUs. A constant energy binning of seven counts per bin was used for Q and U stokes parameters; we required $S/N > 7$ in each channel for the intensity spectra. We then performed a so-called weighted analysis method presented in Di Marco et al. (2022) (parameter STOKES = NEFF in XSELECT) on the resulting spectra. We adopted a circular region with radius 104″ to determine the I, Q, and U Stokes background spectra.

The XMM-Newton scientific products were obtained with the standard science analysis software routines and the latest calibration files. The spectrum of the source was derived using a circular region (radius = 40″) centered on the source. The background was extracted from a blank region on the EPIC-pn CCD camera using a circular region of the same size. The resulting spectrum was rebinned in order to have at least 30 counts in each bin and to avoid oversampling the spectral resolution by a factor >3. The NuSTAR data were calibrated and cleaned using the NuSTAR Data Analysis

[80] http://polami.iaa.es/

[81] https://github.com/WIRC-Pol/wirc_drp

[82] https://people.bu.edu/clemens/mimir/index.html

Table 4
Multiwavelength Polarization Observations Related to the 2022 May IXPE Pointing.

Telescope	X-Ray Flux	Π_X (%)	σ_Π	ψ_X (deg)	σ_ψ
IXPE	0.96 ± 0.03	<14.2	⋯	⋯	⋯
XMM-Newton	0.91 ± 0.02	⋯	⋯	⋯	⋯
NuSTAR	1.14 ± 0.03	⋯	⋯	⋯	⋯
Telescope	Flux density (Jy)	Π_R (%)	σ_Π	ψ_R (deg)	σ_ψ
ALMA (0.87 mm)	5.58 ± 0.26	3.6 ± 0.09	0.3	26 ± 0.9	31
POLAMI (3 mm)	7.78 ± 0.31	4.0 ± 0.39	0.6	30 ± 3	1
POLAMI (1.3 mm)	6.57 ± 1.5	4.2 ± 1.2	0.6	36 ± 7.9	13
Telescope	Magnitude	Π_O (%)	σ_Π	ψ_O (deg)	σ_ψ
AZT-8 and LX-200 (70 and 40 cm)	12.8 ± 0.1	5.0 ± 0.3	3.45	116 ± 2	28
Calar Alto	12.8 ± 0.1	6.8 ± 0.1	2.8	128 ± 1	23
Kanata (*R* band)	⋯	2.49 ± 0.05	0	56.5 ± 0.5	0
Kanata (*J* band)	⋯	3.51 ± 0.05	0	49.0 ± 0.6	0
NOT	⋯	5.9 ± 3.0	3.0	140 ± 28	28
Palomar (*J* band)	⋯	1.70 ± 0.27	0	137 ± 5	0
Palomar (H band)	⋯	0.92 ± 0.15	0	151 ± 5	0
Perkins (H band)	9.69 ± 0.2	4.0 ± 0.4	2.3	86 ± 3	38
Perkins (K band)	8.87 ± 0.2	3.4 ± 2.1	2.1	79 ± 4	37
Sierra Nevada (T150)	12.8 ± 0.2	6.9 ± 0.6	1.8	100 ± 3	46
Skinakas	12.68 ± 0.03	5.77 ± 0.1	0	71 ± 0.5	0
T60	13.28 ± 0.03	4.28 ± 0.09	0	90 ± 1	0

Note. X-ray fluxes correspond to the 2–8 keV energy range and are in units of 10^{-11} erg cm^{-2} s^{-1}. The millimeter-radio flux density is in Janskys (Jy). For the optical observations, we report *R*-band measurements. The infrared observations are affected by the unpolarized host-galaxy contribution to the total light, and so should be treated as lower limits to the true Π. The uncertainties for Π and ψ are either the uncertainty of the measurement or the median uncertainty in the case of multiple measurements; σ_Π and σ_ψ show the standard deviation of the observations.

Table 5
Multwavelength Polarization Observations Related to the 2022 July IXPE Observation

Telescope	X-Ray Flux	Π_X (%)	σ_Π	ψ_X (deg)	σ_ψ
IXPE	1.56 ± 0.06	<12.6	⋯	⋯	⋯
XMM-Newton	1.60 ± 0.01	⋯	⋯	⋯	⋯
Telescope	Flux density (Jy)	Π_R (%)	σ_Π	ψ_R (deg)	σ_ψ
POLAMI (3 mm)	13.7 ± 0.6	5.4 ± 0.5	3.1	15 ± 4	2
POLAMI (1.3 mm)	6.0 ± 0.6	6.1 ± 1.8	1.8	20 ± 9	0.2
SMA (1.3 mm)	7.0 ± 0.7	8.8 ± 1.0	0	19 ± 2	0
Telescope	Magnitude	Π_O (%)	σ_Π	ψ_O (deg)	σ_ψ
Calar Alto	13.9 ± 0.1	15.9 ± 0.1	5.2	40 ± 0.1	7
NOT	⋯	17.0 ± 0.08	0	42 ± 4	0
Sierra Nevada (T90)	13.9 ± 0.01	7.3 ± 0.36	0.2	54 ± 1.4	4
Skinakas	13.26 ± 0.15	13.2 ± 0.1	4.2	38 ± 0.3	5

Note. Same as for Table 4.

Software (NuSTARDAS; Perri et al. 2021[83]), and the scientific products were generated with the *nuproducts* pipeline using the latest calibration database (v. 20220302). The source spectrum was derived using a circular region (radius $= 70''$), and a concentric annulus (r_{in} and r_{out} being $270''$ and $370''$, respectively) was used to derive the background spectrum.

Appendix B
Swift-XRT Observations: Temporal Behavior of BL Lac

Wehere report on a list of the Swift-XRT exposures that were obtained in the context of a monitoring campaign aimed at tracking the flux level of BL Lac. Scientific products from the Swift-XRT exposures were derived using the facilities provided by the Space Science Data Center (SSDC[84]) of the Italian Space Agency (ASI). In particular, the source spectra were extracted with a circular region of radius $\sim 47''$, with a concentric annulus for determination of the background with inner (outer) radii of 120 (150) arcseconds. The spectra were then binned in order to include at least 25 counts in each bin. We modeled each of the obtained 21 XRT spectra as a simple power law with Galactic photoelectric absorption. This model was found to adequately reproduce the data, based on the χ^2 statistic. We report the 2–8 keV fluxes and the inferred photon indices in Table 6. We then used Swift light curve to study the variability properties of BL Lac over ~ 3 months preceding and including the dates in which IXPE was observing BL Lac. The photon index as well as the 2–8 keV flux of BL Lac was derived for each of the XRT exposures fitting a simple power law observed for the Galaxy. Our results, quoted in Table 6, are in agreement with a harder when brighter behavior as the 2–8 flux and Γ are moderately anticorrelated with a Pearson cross-correlation coefficient of $P_{cc} = -0.6$ and an accompanying null probability $P(<r) = 0.004$. This behavior has been already observed in blazars and BL Lac itself (e.g., Prince 2021) and is suggestive of a nonflaring activity of the source. Interestingly, this anticorrelation is moderately stronger if we consider the

[83] https://heasarc.gsfc.nasa.gov/docs/nustar/analysis/nustar_swguide.pdf

[84] https://www.ssdc.asi.it/

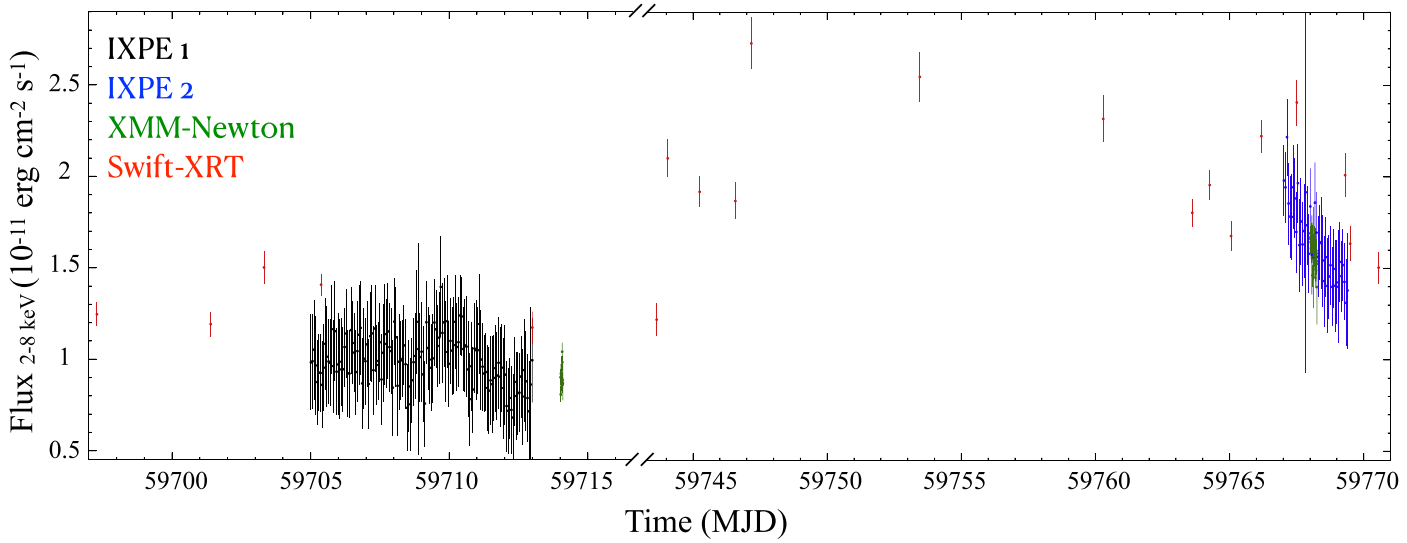

Figure 5. Multimission light curve of BL Lac as observed in the 2–8 keV energy range. Different colors account for the various facilities. No significant intraobservation variability is observed during the first IXPE pointing, while, a flux decrease by a factor of ∼30% is observed during the second exposure.

Table 6
The Swift-XRT Observations Belonging to BL Lac Monitoring Campaign Before, During, and After the Two IXPE Observations

Start Time (yyyy-mm-dd hh:mm:ss)	Time (MJD)	ObsID	$\mathrm{Flux}_{2-8\ \mathrm{keV}}$ (10^{-11} erg cm^{-2} s^{-1})	Γ
2022-04-28 06:55:35	59697.288	00096565001	1.24 ± 0.06	1.54 ± 0.15
2022-05-02 09:27:36	59701.394	00096565002	1.19 ± 0.06	1.69 ± 0.15
2022-05-04 07:36:35	59703.317	00096565003	1.50 ± 0.09	1.56 ± 0.16
2022-05-06 09:01:35	59705.376	00089271001	1.40 ± 0.15	1.57 ± 0.11
2022-05-13 23:57:35	59712.998	00096565004	1.17 ± 0.08	1.36 ± 0.22
2022-06-12 18:40:35	59742.778	00014925008	1.35 ± 0.09	1.56 ± 0.18
2022-06-13 15:21:45	59743.640	00014925009	1.22 ± 0.08	1.53 ± 0.22
2022-06-14 01:16:35	59744.053	00014925010	2.10 ± 0.10	1.25 ± 0.17
2022-06-15 05:50:35	59745.243	00014925011	1.91 ± 0.08	1.45 ± 0.13
2022-06-16 13:47:34	59746.574	00014925012	1.86 ± 0.09	1.33 ± 0.17
2022-06-17 04:04:35	59747.169	00014925013	2.73 ± 0.14	1.44 ± 0.15
2022-06-23 10:51:36	59753.452	00096990001	2.54 ± 0.13	1.26 ± 0.16
2022-06-30 06:56:36	59760.289	00096990002	2.31 ± 0.12	1.49 ± 0.16
2022-07-03 14:38:35	59763.610	00096990003	1.80 ± 0.07	1.35 ± 0.13
2022-07-04 06:13:38	59764.259	00096990004	1.96 ± 0.08	1.45 ± 0.12
2022-07-05 01:17:37	59765.054	00096990005	1.67 ± 0.07	1.36 ± 0.15
2022-07-06 04:23:36	59766.183	00096990006	2.22 ± 0.08	1.40 ± 0.12
2022-07-07 12:09:37	59767.506	00096990007	2.40 ± 0.12	1.28 ± 0.17
2022-07-09 07:22:36	59769.307	00096990008	2.01 ± 0.11	1.36 ± 0.19
2022-07-09 11:54:36	59769.496	00096990009	1.63 ± 0.09	1.55 ± 0.16
2022-07-10 13:21:36	59770.556	00096990010	1.50 ± 0.08	1.55 ± 0.16

2–10 keV flux ($P_{cc} = -0.64$ and $P(<r) = 0.002$), while no relation between the photon index and 0.5–2 keV flux is found in this data set. Finally, in Figure 5, we report the flux variability and compare it with the two IXPE and XMM-Newton light curves.

ORCID iDs

Riccardo Middei https://orcid.org/0000-0001-9815-9092
Ioannis Liodakis https://orcid.org/0000-0001-9200-4006
Matteo Perri https://orcid.org/0000-0003-3613-4409
Simonetta Puccetti https://orcid.org/0000-0002-2734-7835
Elisabetta Cavazzuti https://orcid.org/0000-0001-7150-9638
Laura Di Gesu https://orcid.org/0000-0000-0000-0000
Steven R. Ehlert https://orcid.org/0000-0003-1111-4292
Alan P. Marscher https://orcid.org/0000-0001-7396-3332
Herman L. Marshall https://orcid.org/0000-0002-6492-1293
Fabio Muleri https://orcid.org/0000-0003-3331-3794
Michela Negro https://orcid.org/0000-0002-6548-5622
Svetlana G. Jorstad https://orcid.org/0000-0001-6158-1708
Beatriz Agís-González https://orcid.org/0000-0001-7702-8931
Iván Agudo https://orcid.org/0000-0002-3777-6182
Giacomo Bonnoli https://orcid.org/0000-0003-2464-9077
César Husillos https://orcid.org/0000-0001-8286-5443
Alessandro Marchini https://orcid.org/0000-0003-3779-6762
Pouya M. Kouch https://orcid.org/0000-0002-9328-2750
Evgenia N. Kopatskaya https://orcid.org/0000-0001-9518-337X

Elena G. Larionova https://orcid.org/0000-0002-2471-6500
Sergey S. Savchenko https://orcid.org/0000-0003-4147-3851
Andrey A. Vasilyev https://orcid.org/0000-0002-8293-0214
Carolina Casadio https://orcid.org/0000-0003-1117-2863
Juan Escudero https://orcid.org/0000-0002-4131-655X
Ioannis Myserlis https://orcid.org/0000-0003-3025-9497
Seiji Kameno https://orcid.org/0000-0002-5158-0063
Ruediger Kneissl https://orcid.org/0000-0002-5580-006X
Hiroshi Nagai https://orcid.org/0000-0003-0292-3645
Dmitry Blinov https://orcid.org/0000-0002-8597-6154
Ioakeim G. Bourbah https://orcid.org/0000-0002-8597-6154
Sebastian Kiehlmann https://orcid.org/0000-0001-6314-9177
Nikos Mandarakas https://orcid.org/0000-0002-2567-2132
Stylianos Romanopoulos https://orcid.org/0000-0002-2897-2448
Raphael Skalidis https://orcid.org/0000-0003-2337-0277
Joseph R. Masiero https://orcid.org/0000-0003-2638-720X
Dimitri Mawet https://orcid.org/0000-0002-8895-4735
Maxwell A. Millar-Blanchaer https://orcid.org/0000-0001-6205-9233
Georgia V. Panopoulou https://orcid.org/0000-0001-7482-5759
Samaporn Tinyanont https://orcid.org/0000-0002-1481-4676
Andrei V. Berdyugin https://orcid.org/0000-0002-9353-5164
Vadim Kravtsov https://orcid.org/0000-0002-7502-3173
Ryo Imazawa https://orcid.org/0000-0002-0643-7946
Yasushi Fukazawa https://orcid.org/0000-0002-0921-8837
Koji S. Kawabata https://orcid.org/0000-0001-6099-9539
Makoto Uemura https://orcid.org/0000-0002-7375-7405
Tsunefumi Mizuno https://orcid.org/0000-0001-7263-0296
Hiroshi Akitaya https://orcid.org/0000-0001-6156-238X
Mark Gurwell https://orcid.org/0000-0003-0685-3621
Niccoló Di Lalla https://orcid.org/0000-0002-7574-1298
Nicoló Cibrario https://orcid.org/0000-0003-3842-4493
Immacolata Donnarumma https://orcid.org/0000-0002-4700-4549
Dawoon E. Kim https://orcid.org/0000-0001-5717-3736
Nicola Omodei https://orcid.org/0000-0002-5448-7577
Luigi Pacciani https://orcid.org/0000-0001-6897-5996
Juri Poutanen https://orcid.org/0000-0002-0983-0049
Fabrizio Tavecchio https://orcid.org/0000-0003-0256-0995
Lucio A. Antonelli https://orcid.org/0000-0002-5037-9034
Matteo Bachetti https://orcid.org/0000-0002-4576-9337
Luca Baldini https://orcid.org/0000-0002-9785-7726
Wayne H. Baumgartner https://orcid.org/0000-0002-5106-0463
Ronaldo Bellazzini https://orcid.org/0000-0002-2469-7063
Stefano Bianchi https://orcid.org/0000-0002-4622-4240
Stephen D. Bongiorno https://orcid.org/0000-0002-0901-2097
Raffaella Bonino https://orcid.org/0000-0002-4264-1215
Alessandro Brez https://orcid.org/0000-0002-9460-1821
Niccoló Bucciantini https://orcid.org/0000-0002-8848-1392
Fiamma Capitanio https://orcid.org/0000-0002-6384-3027
Simone Castellano https://orcid.org/0000-0003-1111-4292
Stefano Ciprini https://orcid.org/0000-0002-0712-2479
Enrico Costa https://orcid.org/0000-0003-4925-8523
Alessandra De Rosa https://orcid.org/0000-0001-5668-6863
Ettore Del Monte https://orcid.org/0000-0002-3013-6334
Alessandro Di Marco https://orcid.org/0000-0003-0331-3259
Victor Doroshenko https://orcid.org/0000-0001-8162-1105
Michal Dovčiak https://orcid.org/0000-0003-0079-1239
Teruaki Enoto https://orcid.org/0000-0003-1244-3100
Yuri Evangelista https://orcid.org/0000-0001-6096-6710
Sergio Fabiani https://orcid.org/0000-0003-1533-0283
Riccardo Ferrazzoli https://orcid.org/0000-0003-1074-8605
Javier A. Garcia https://orcid.org/0000-0003-3828-2448
Shuichi Gunji https://orcid.org/0000-0002-5881-2445
Jeremy Heyl https://orcid.org/0000-0001-9739-367X
Wataru Iwakiri https://orcid.org/0000-0002-0207-9010
Vladimir Karas https://orcid.org/0000-0002-5760-0459
Jeffery J. Kolodziejczak https://orcid.org/0000-0002-0110-6136
Henric Krawczynski https://orcid.org/0000-0002-1084-6507
Fabio La Monaca https://orcid.org/0000-0001-8916-4156
Luca Latronico https://orcid.org/0000-0002-0984-1856
Simone Maldera https://orcid.org/0000-0002-0698-4421
Alberto Manfreda https://orcid.org/0000-0002-0998-4953
Frédéric Marin https://orcid.org/0000-0003-4952-0835
Andrea Marinucci https://orcid.org/0000-0002-2055-4946
Francesco Massaro https://orcid.org/0000-0002-1704-9850
Giorgio Matt https://orcid.org/0000-0002-2152-0916
C.-Y. Ng https://orcid.org/0000-0002-5847-2612
Stephen L. O'Dell https://orcid.org/0000-0002-1868-8056
Chiara Oppedisano https://orcid.org/0000-0001-6194-4601
Alessandro Papitto https://orcid.org/0000-0001-6289-7413
George G. Pavlov https://orcid.org/0000-0002-7481-5259
Abel L. Peirson https://orcid.org/0000-0001-6292-1911
Melissa Pesce-Rollins https://orcid.org/0000-0003-1790-8018
Pierre-Olivier Petrucci https://orcid.org/0000-0001-6061-3480
Maura Pilia https://orcid.org/0000-0001-7397-8091
Andrea Possenti https://orcid.org/0000-0001-5902-3731
John Rankin https://orcid.org/0000-0002-9774-0560
Ajay Ratheesh https://orcid.org/0000-0003-0411-4243
Roger W. Romani https://orcid.org/0000-0001-6711-3286
Carmelo Sgró https://orcid.org/0000-0001-5676-6214
Patrick Slane https://orcid.org/0000-0002-6986-6756
Paolo Soffitta https://orcid.org/0000-0001-8916-4156
Gloria Spandre https://orcid.org/0000-0003-0802-3453
Toru Tamagawa https://orcid.org/0000-0002-8801-6263
Roberto Taverna https://orcid.org/0000-0002-1768-618X
Allyn F. Tennant https://orcid.org/0000-0002-9443-6774
Nicholas E. Thomas https://orcid.org/0000-0003-0411-4606
Francesco Tombesi https://orcid.org/0000-0002-6562-8654
Alessio Trois https://orcid.org/0000-0002-3180-6002
Sergey Tsygankov https://orcid.org/0000-0002-9679-0793
Roberto Turolla https://orcid.org/0000-0003-3977-8760
Jacco Vink https://orcid.org/0000-0002-4708-4219
Martin C. Weisskopf https://orcid.org/0000-0002-5270-4240
Kinwah Wu https://orcid.org/0000-0002-7568-8765
Fei Xie https://orcid.org/0000-0002-0105-5826
Silvia Zane https://orcid.org/0000-0001-5326-880X

References

Abdo, A. A., Ackermann, M., Ajello, M., et al. 2011, ApJ, 730, 101
Agudo, I., Jorstad, S. G., Marscher, A. P., et al. 2011a, ApJL, 726, L13
Agudo, I., Marscher, A. P., Jorstad, S. G., et al. 2011b, ApJL, 735, L10
Agudo, I., Thum, C., Molina, S. N., et al. 2018a, MNRAS, 474, 1427
Agudo, I., Thum, C., Ramakrishnan, V., et al. 2018b, MNRAS, 473, 1850

Ajello, M., Angioni, R., Axelsson, M., et al. 2020, ApJ, 892, 105
Akitaya, H., Moritani, Y., Ui, T., et al. 2014, Proc. SPIE, 9147, 91474O
Albert, J., Aliu, E., Anderhub, H., et al. 2007, ApJL, 666, L17
Arlen, T., Aune, T., Beilicke, M., et al. 2013, ApJ, 762, 92
Bania, T. M., Marscher, A. P., & Barvainis, R. 1991, AJ, 101, 2147
Begelman, M. C., Sikora, M., Giommi, P., et al. 1987, ApJ, 322, 650
Berdyugin, A., Piirola, V., & Poutanen, J. 2019, in Astrophysics and Space Science Library, Astronomical Polarisation from the Infrared to Gamma Rays, ed. R. Shearer et al., Vol. 460 (Cham: Springer), 33
Berdyugin, A. V., Berdyugina, S. V., & Piirola, V. 2018, Proc. SPIE, 10702, 107024Z
Blandford, R., Meier, D., & Readhead, A. 2019, ARA&A, 57, 467
Blinov, D., Kiehlmann, S., Pavlidou, V., et al. 2021, MNRAS, 501, 3715
Blinov, D., Pavlidou, V., Papadakis, I., et al. 2015, MNRAS, 453, 1669
Blinov, D., Pavlidou, V., Papadakis, I., et al. 2018, MNRAS, 474, 1296
Bonometto, S., & Saggion, A. 1973, A&A, 23, 9
Böttcher, M., & Bloom, S. D. 2000, AJ, 119, 469
Böttcher, M., Reimer, A., Sweeney, K., & Prakash, A. 2013, ApJ, 768, 54
Bradley, L., Sipocz, B., Robitaille, T., et al. 2019, astropy/photutils: v0.6, Zenodo, doi:10.5281/zenodo.2533376
Burrows, D. N., Hill, J. E., Nousek, J. A., et al. 2005, SSRv, 120, 165
Casadio, C., MacDonald, N. R., Boccardi, B., et al. 2021, A&A, 649, A153
Cerruti, M., Zech, A., Boisson, C., & Inoue, S. 2015, MNRAS, 448, 910
Cerruti, M., Benbow, W., Chen, X., et al. 2017, A&A, 606, 10
Clemens, D. P., Pinnick, A. F., & Pavel, M. D. 2012, ApJS, 200, 20
Di Gesu, L., Donnarumma, I., Tavecchio, F., et al. 2022, ApJL, 938, L7
Di Marco, A., Costa, E., Muleri, F., et al. 2022, AJ, 163, 170
Giommi, P., Perri, M., Capalbi, M., et al. 2021, MNRAS, 507, 5690
Harrison, F. A., Craig, W. W., Christensen, F. E., et al. 2013, ApJ, 770, 103
Hovatta, T., & Lindfors, E. 2019, NewAR, 87, 101541
Hovatta, T., Lindfors, E., Blinov, D., et al. 2016, A&A, 596, A78
IceCube Collaboration, Aartsen, M. G., Ackermann, M., et al. 2018, Sci, 361, eaat1378
Jansen, F., Lumb, D., Altieri, B., et al. 2001, A&A, 365, L1
Kawabata, K. S., Okazaki, A., Akitaya, H., et al. 1999, PASP, 111, 898
Kosenkov, I. A., Berdyugin, A. V., Piirola, V., et al. 2017, MNRAS, 468, 4362
Liodakis, I., Blinov, D., Potter, S. B., & Rieger, F. M. 2022a, MNRAS, 509, L21
Liodakis, I., Marscher, A. P., Agudo, I., et al. 2022b, Natur, 611, 677
Liodakis, I., Peirson, A. L., & Romani, R. W. 2019a, ApJ, 880, 29
Liodakis, I., & Petropoulou, M. 2020, ApJL, 893, L20
Liodakis, I., Romani, R. W., Filippenko, A. V., et al. 2018, MNRAS, 480, 5517
Liodakis, I., Romani, R. W., Filippenko, A. V., Kocevski, D., & Zheng, W. 2019b, ApJ, 880, 32
Madejski, G. M., Sikora, M., Jaffe, T., et al. 1999, ApJ, 521, 145
MAGIC Collaboration, Acciari, V. A., Ansoldi, S., et al. 2019, A&A, 623, A175
Marscher, A. P. 2014, ApJ, 780, 87
Marscher, A. P., Jorstad, S. G., D'Arcangelo, F. D., et al. 2008, Natur, 452, 966
Masiero, J. R., Tinyanont, S., & Millar-Blanchaer, M. A. 2022, PSJ, 3, 90
Middei, R., Giommi, P., Perri, M., et al. 2022, MNRAS, 514, 3179
Millar-Blanchaer, M. A., Tinyanont, S., Jovanovic, N., et al. 2021, Proc. SPIE, 11447, 1315
Morris, P. J., Potter, W. J., & Cotter, G. 2019, MNRAS, 486, 1548
Nagirner, D. I., & Poutanen, J. 1993, A&A, 275, 325
Nilsson, K., Lindfors, E., Takalo, L. O., et al. 2018, A&A, 620, A185
Paliya, V. S., Zhang, H., Bottcher, M., et al. 2018, ApJ, 863, 98
Panopoulou, G., Tassis, K., Blinov, D., et al. 2015, MNRAS, 452, 715
Peirson, A. L., & Romani, R. W. 2019, ApJ, 885, 76
Perri, M., Puccetti, S., Spagnuolo, N., et al. 2021, SSDC-ASI/NASA, V. 1.9.7, https://heasarc.gsfc.nasa.gov/docs/nustar/analysis/nustar_swguide.pdf
Piirola, V. 1973, A&A, 27, 383
Piirola, V., Berdyugin, A., & Berdyugina, S. 2014, Proc. SPIE, 9147, 91478I
Piirola, V., Kosenkov, I. A., Berdyugin, A. V., Berdyugina, S. V., & Poutanen, J. 2021, AJ, 161, 20
Poutanen, J. 1994, ApJS, 92, 607
Prince, R. 2021, MNRAS, 507, 5602
Raiteri, C. M., Villata, M., D'Ammando, F., et al. 2013, MNRAS, 436, 1530
Ramaprakash, A. N., Rajarshi, C. V., Das, H. K., et al. 2019, MNRAS, 485, 2355
Sahakyan, N., & Giommi, P. 2022, MNRAS, 513, 4645
Struder, L., Briel, U., Dennerl, K., et al. 2001, A&A, 365, L18
Tavecchio, F., Landoni, M., Sironi, L., & Coppi, P. 2018, MNRAS, 480, 2872
Thum, C., Agudo, I., Molina, S. N., et al. 2018, MNRAS, 473, 2506
Tinyanont, S., Millar-Blanchaer, M., Jovanovic, N., et al. 2019a, Proc. SPIE, 11132, 1113209
Tinyanont, S., Millar-Blanchaer, M. A., Nilsson, R., et al. 2019b, PASP, 131, 025001
Vermeulen, R. C., Ogle, P. M., Tran, H. D., et al. 1995, ApJL, 452, L5
Wardle, J. F. C., Homan, D. C., Ojha, R., & Roberts, D. H. 1998, Natur, 395, 457
Weaver, Z. R., Jorstad, S. G., Marscher, A. P., et al. 2022, ApJS, 260, 12
Weaver, Z. R., Williamson, K. E., Jorstad, S. G., et al. 2020, ApJ, 900, 137
Wehrle, A. E., Grupe, D., Jorstad, S. G., et al. 2016, ApJ, 816, 53
Weisskopf, M. C., Elsner, R. F., & O'Dell, S. L. 2010, Proc. SPIE, 7732, 77320E
Weisskopf, M. C., Ramsey, B., O'Dell, S., et al. 2016, Proc. SPIE, 9905, 990517
Weisskopf, M. C., Soffitta, P., Baldini, L., et al. 2022, JATIS, 8, 026002
Zdziarski, A. A., & Bottcher, M. 2015, MNRAS, 450, L21
Zhang, H., & Bottcher, M. 2013, ApJ, 774, 18
Zhang, H., Diltz, C., & Bottcher, M. 2016, ApJ, 829, 69
Zhang, H., Fang, K., Li, H., et al. 2019, ApJ, 876, 109